

Investigation into Phase Diagrams of the Fluorine–Oxygen System: Ferroelastic–Antiferroelectric $(\text{NH}_4)_2\text{WO}_2\text{F}_4$ – $(\text{NH}_4)_2\text{MoO}_2\text{F}_4$

E. V. Bogdanov^{a, d, *}, E. I. Pogoreltsev^{a, b}, S. V. Mel'nikova^a, M. V. Gorev^{a, b}, I. N. Flerov^{a, b},
M. S. Molochev^a, A. V. Kartashev^a, A. G. Kocharova^a, and N. M. Laptash^c

^a Kirensky Institute of Physics, Siberian Branch, Russian Academy of Sciences, Akademgorodok, Krasnoyarsk, 660036 Russia

* e-mail: evbogdanov@iph.krasn.ru

^b Institute of Engineering Physics and Radioelectronics, Siberian Federal University,
ul. Kirenskogo 28, Krasnoyarsk, 660074 Russia

^c Institute of Chemistry, Far Eastern Branch, Russian Academy of Sciences,
pr. Stoletiya Vladivostoka 159, Vladivostok, 690022 Russia

^d Institute of Energetics and Power Resources Management, Krasnoyarsk State Agricultural University,
pr. Mira 90, Krasnoyarsk, 660049 Russia

Received July 10, 2012

Abstract—Thermal, physical, structural, optical, and dielectric investigations have been performed for oxyfluoride solid solutions $(\text{NH}_4)_2\text{W}_{1-x}\text{Mo}_x\text{O}_2\text{F}_4$ ($x = 0, 0.1, 0.2, 0.3, 0.4, 0.6, 0.8, 1$). The character of the influence of the chemical and hydrostatic pressures on the stability of the parent (space group *Cmcm*) and distorted ferroelastic and antiferroelectric phases has been determined by analyzing the temperature–pressure, unit cell volume–composition, and temperature–composition phase diagrams. The specific features of the nature and mechanism of the phase transitions have been discussed using the available data on the structural, entropy, and dielectric parameters.

DOI: 10.1134/S1063783413020042

1. INTRODUCTION

The presence of fluorine–oxygen anion polyhedra in the crystal lattice, namely, $[\text{MeO}_3\text{F}_3]^{n-}$, $[\text{MeO}_2\text{F}_4]^{n-}$, or $[\text{MeOF}_5]^{n-}$, in which the central atom is displaced toward the direction of the oxygen atoms, makes it possible to obtain polar materials with ferroelectric, pyroelectric, or piezoelectric properties [1, 2]. These properties can exhibit themselves as a result of the ordering of structural elements that occurs either in the parent phase after the crystallization [3] or in distorted phases formed upon the phase transformations. However, the low-temperature phases of oxyfluorides often also have a centrosymmetric structure. This situation is observed, for example, in the $(\text{NH}_4)_2\text{MeO}_2\text{F}_4$ ($\text{Me} = \text{W}, \text{Mo}$) compounds with the parent orthorhombic structure (space group *Cmcm*, $Z = 4$), which consists of isolated octahedra $[\text{MeO}_2\text{F}_4]^{2-}$ and two crystallographically nonequivalent ammonium groups [4, 5]. Despite the small difference between the ionic radii of the central atoms (0.59 Å for Mo and 0.60 Å for W), their individual features exerted an influence on the character of the disordering of the octahedra. Accordingly, the probabilities of the occupation of two crystallographic positions 4(c) and 16(h) by these atoms proved to be different: 0.143(6) and 0.214(2) for the $[\text{WO}_2\text{F}_4]^{2-}$ octahedron and 0.43(6) and 0.14(2) for the $[\text{MoO}_2\text{F}_4]^{2-}$ octahedron, respectively.

Detailed investigations of the $(\text{NH}_4)_2\text{WO}_2\text{F}_4$ oxyfluoride have demonstrated that, at the temperature $T_1 = 201$ K, the parent structure of this oxyfluoride loses its stability [6, 7]. The absence of the second harmonic generation below the temperature T_1 indicates that the structure has the center of symmetry, while the character of the optical twinning suggests a ferroelastic nature of the structural phase transition that occurs with the symmetry change $\text{Cmcm} \leftrightarrow P\bar{1}$. The distortion of the parent structure results in a complete ordering of fluorine–oxygen octahedra; however, the ammonium groups remain partially disordered [4, 5]. The investigations of the temperature dependences of the heat capacity and susceptibility to hydrostatic pressure have shown that the aforementioned phase transition is a first-order transformation, which is characterized by a significant change in the entropy $\Delta S_1 = R \ln 9.8$ and a small pressure coefficient $dT_1/dp = 13.4$ K/GPa. Based on the model of the structure distortion and the results of the study of the deuterated compound $(\text{ND}_4)_2\text{WO}_2\text{F}_4$, it was concluded that the dominant contribution to the entropy change ΔS_1 comes from the ordering of the $[\text{WO}_2\text{F}_4]^{2-}$ anions [8].

The substitution for the central atom $\text{Mo} \rightarrow \text{W}$ in the structure leads to a sharp increase in the temperature of loss in the stability of the parent phase (space

group *Cmcm*), i.e., $T_1 = 270$ K, as well as to a change in the symmetry of the distorted phase (space group *Prma*, $Z = 4$), which proves to be antiferroelectric [5, 9, 10]. A significant difference between $(\text{NH}_4)_2\text{WO}_2\text{F}_4$ and $(\text{NH}_4)_2\text{MoO}_2\text{F}_4$ lies in the fact that, in the former compound below the temperature T_1 , there occurs a complete ordering of two nonequivalent ammonium groups, i.e., all the hydrogen atoms are localized; however, the fluorine–oxygen octahedra remain partially disordered. The phase transition in the $(\text{NH}_4)_2\text{MoO}_2\text{F}_4$ oxyfluoride at the temperature T_1 remains a first-order transformation of the order–disorder type ($\Delta S_1 = R \ln 8.9$). In this case, the pressure coefficient increases by a factor of almost seven, i.e., $dT_1/dp = 92.7$ K/GPa. The dominant contribution to the entropy of the phase transition is associated with a partial ordering of the $[\text{MoO}_2\text{F}_4]^{2-}$ anions, which is confirmed, in particular, by the results obtained from the analysis of the role played by the monovalent cation in the $(\text{NH}_4)_{2-x}A_x\text{MoO}_2\text{F}_4$ ($A = \text{K}, \text{Rb}, \text{Cs}$) solid solutions used as an example [11]. The partial substitution of the spherical cation for the tetrahedral cation makes it possible to control the order of the phase transition and the limits of stability of the parent phase (space group *Cmcm*) with respect to changes in both the temperature and the pressure. This leads to a significant decrease in the entropy change. For example, in $\text{Rb}_2\text{MoO}_2\text{F}_4$ and $(\text{NH}_4)_2\text{MoO}_2\text{F}_4$, the entropy changes ΔS_1 are in the ratio of 9.2/18.2. This value indicates that the ammonium cation plays an important role in the mechanism of phase transition of the order–disorder type. However, the entropy change in the rubidium oxyfluoride is still rather large; therefore, the parent structure also remains disordered in the absence of the tetrahedral cation in the crystal lattice.

It has been found that, in the low-temperature range at the temperature T_2 , all the studied compounds $(\text{NH}_4)_{2-x}A_x\text{MeO}_2\text{F}_4$ also exhibit an anomalous behavior of the heat capacity $C_p(T)$, thermal expansion $\beta(T)$, permittivity $\varepsilon(T)$, and birefringence $\Delta n(T)$ [6–12]. Since the X-ray diffraction patterns recorded below the temperature T_2 do not exhibit any changes [4, 5], it can be assumed that the low-temperature transformation, most likely, is associated with very small displacements of any structural elements.

In this work, we have performed investigations of the temperature–composition, unit cell volume–composition, and temperature–pressure phase diagrams for a system of solid solutions $(\text{NH}_4)_2\text{W}_{1-x}\text{Mo}_x\text{O}_2\text{F}_4$ in order to elucidate in more detail the role played by the central atom in the mechanism and nature of the phase transitions in oxyfluorides with orthorhombic symmetry (space group *Cmcm*). For this purpose, we have examined the heat capacity, entropy, thermal expansion, susceptibility to external pressure, permittivity, and birefringence.

2. SYNTHESIS, GROWTH, AND STRUCTURE OF THE CRYSTALS

The solid solutions $(\text{NH}_4)_2\text{W}_{1-x}\text{Mo}_x\text{O}_2\text{F}_4$ ($x = 0.2, 0.4, 0.6, 0.8$) were synthesized from the corresponding stoichiometric weighed portions of the initial ammonium oxofluorometallates $(\text{NH}_4)_2\text{MoO}_2\text{F}_4$ and $(\text{NH}_4)_2\text{WO}_2\text{F}_4$; the procedure used for their growth in the form of single crystals was described in detail in [4, 5].

A mixture of the initial components in required ratios (the weight of the mixture was 10–15 g) was dissolved in water with the addition of a few drops of a concentrated hydrofluoric acid HF (40%) in order to prevent hydrolysis. The solution was gently evaporated on a water bath and then filtered out. Later, the spontaneous crystallization proceeded through a slow evaporation of the solution in air.

The composition of the grown crystals was controlled by the molybdenum and tungsten concentrations, which were determined using the atomic absorption method. It should be noted that, for $x = 0.2$, the actual composition of the crystals (within the error of the analysis) corresponded to $x = 0.180$ – 0.185 . In the case of $x = 0.8$, the results of the analysis were close to the calculated composition.

Crystals with $x = 0.1$ and 0.3 were grown by mixing the ammonium tungstate $(\text{NH}_4)_{10}\text{W}_{12}\text{O}_{41} \cdot \text{H}_2\text{O}$ with hydrofluoric acid HF in required stoichiometric amounts. The obtained colorless crystals of $\text{NH}_4[\text{W}_x\text{O}_2\text{F}_3] \cdot \text{H}_2\text{O}$ were dissolved in ammonia water NH_4OH with the addition of the molybdenum oxide Mo_xO_3 and hydrofluoric acid HF in appropriate proportions. The slow evaporation in air resulted in the formation of single crystals of the $(\text{NH}_4)_2\text{W}_{1-x}\text{Mo}_x\text{O}_2\text{F}_4$ ($x = 0.1, 0.3$) solid solutions.

The linear dimensions of the single crystals obtained by different methods were varied in the range 0.1–5.0 mm. Therefore, the X-ray diffraction investigations were performed on two types of diffractometers, namely, a D8 Advance Bruker powder diffractometer and a Smart Apex II single-crystal diffractometer. At room temperature, all the solid solutions, as well as the parent oxyfluorides, are characterized by the orthorhombic symmetry (space group *Cmcm*). The concentration dependences of the unit cell parameters are shown in Fig. 1. It has been found that the successive substitution $\text{Mo} \rightarrow \text{W}$ is accompanied by a non-linear change in all the parameters under investigation. In the first stage, the derivatives da/dx , db/dx , and dc/dx are negative in the composition region with a molybdenum concentration $x \leq 0.2$. With a further increase in the molybdenum concentration, the unit cell parameters a and c increase, whereas the parameter b decreases. In the refinement of the structure, we determined the actual composition of the solid solutions, which, in the majority of cases, was very close (± 0.01) to the composition determined by the chemical analysis.

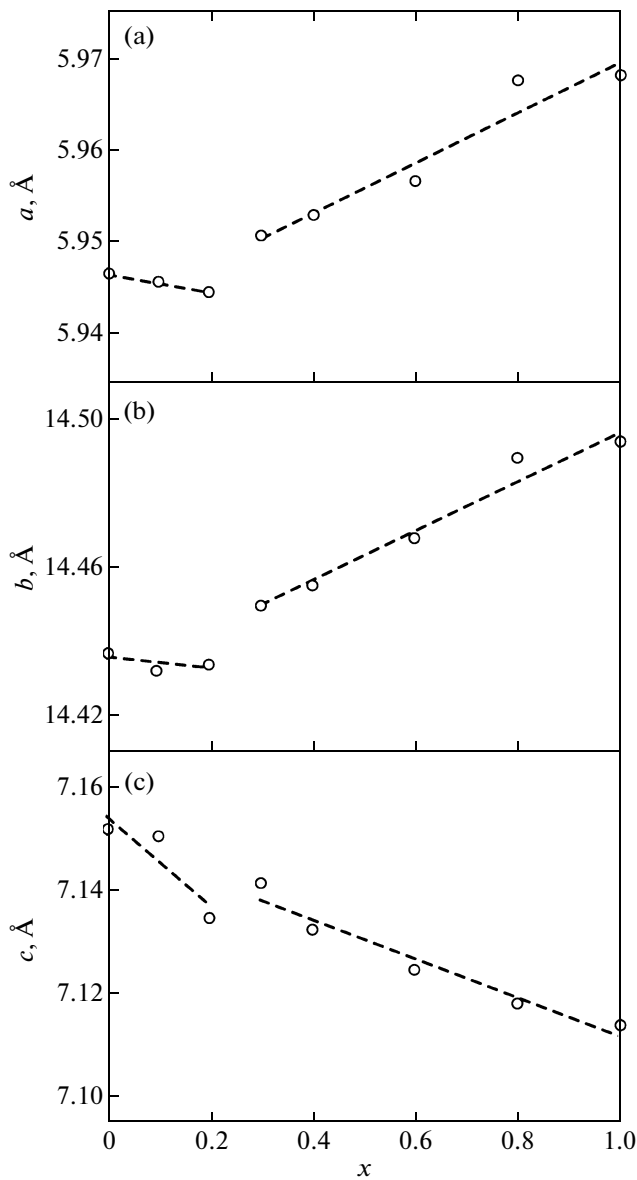


Fig. 1. Concentration dependences of the unit cell parameters of the $(\text{NH}_4)_2\text{W}_{1-x}\text{Mo}_x\text{O}_2\text{F}_4$ single crystals.

The elemental composition of the $(\text{NH}_4)_2\text{W}_{1-x}\text{Mo}_x\text{O}_2\text{F}_4$ ($x = 0.2, 0.3, 0.4$) compounds was determined using the X-ray fluorescence analysis on an S4 Pioneer wavelength dispersive X-ray fluorescence spectrometer (Bruker). We achieved a satisfactory agreement between the experimentally determined concentrations of individual elements and their concentrations calculated from the chemical formula.

3. HEAT CAPACITY, THERMAL EXPANSION, AND T - p PHASE DIAGRAM

All the synthesized solid solutions $(\text{NH}_4)_2\text{W}_{1-x}\text{Mo}_x\text{O}_2\text{F}_4$, including the parent oxyfluorides, were investigated using a DSM-10 differential

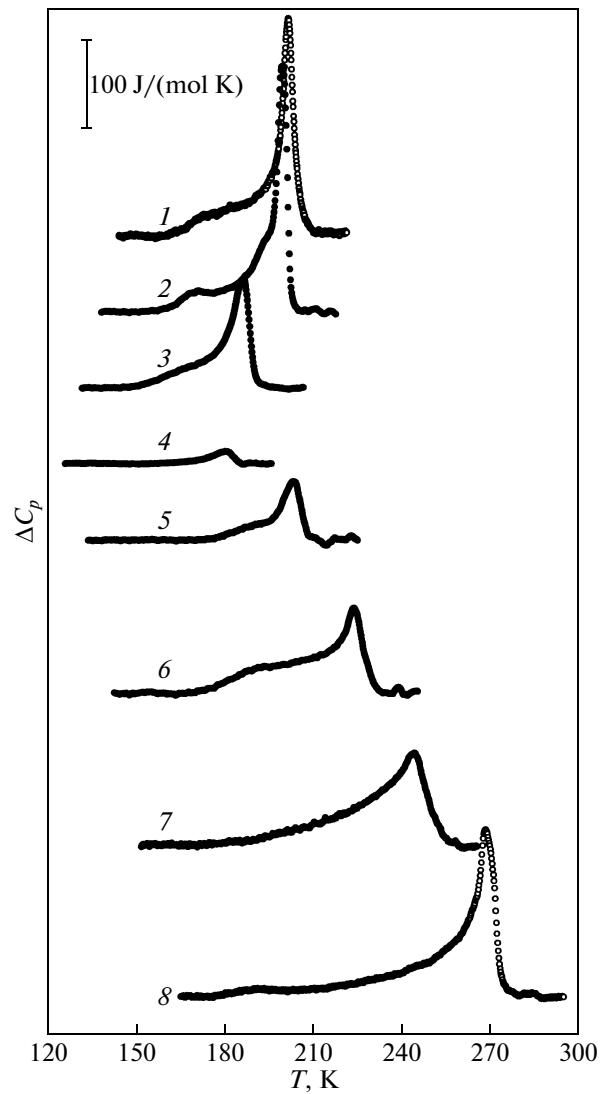


Fig. 2. Temperature dependences of the anomalous heat capacity $\Delta C_p(T)$ for (1) $(\text{NH}_4)_2\text{WO}_2\text{F}_4$; (2–7) $(\text{NH}_4)_2\text{W}_{1-x}\text{Mo}_x\text{O}_2\text{F}_4$ with $x =$ (2) 0.1, (3) 0.2, (4) 0.3, (5) 0.4, (6) 0.6, and (7) 0.8; and (8) $(\text{NH}_4)_2\text{MoO}_2\text{F}_4$.

scanning microcalorimeter (DSM) in order to obtain information about the occurrence of phase transitions, their temperatures, heat capacity, and integral energy parameters. The measurements were performed over a wide temperature range 120–400 K at a rate of 8 K/min during heating and cooling of the samples weighing as much as ~ 0.2 g.

It has been found that the heat capacity of all the samples under investigation is characterized by an anomalous behavior at two characteristic temperatures due to the sequence of two phase transformations. In the future, we will be interested only in the thermal and physical parameters associated with structural distortions. For this reason, in Fig. 2 we presented the temperature dependences of the anomalous heat capacity $\Delta C_p(T)$. In order to determine the anom-

Thermodynamic parameters of the successive phase transitions at the temperatures T_1 and T_2 in the $(\text{NH}_4)_2\text{W}_{1-x}\text{Mo}_x\text{O}_2\text{F}_4$ solid solutions according to the data obtained from the DSM investigations

x	T_1 , K	T_2 , K	$\Sigma\Delta H_i$, J/(mol K)	$\Sigma\Delta S_i$, J/(mol K)	dT_1/dp , K/GPa	dT_2/dp , K/GPa
0	201.2	160	2690	13.8	13.4 [6]	41.7 [6]
0.1	199.1	170.1	2600	13.3	—	—
0.2	186.2	165	1980	9.8	3.0	-210.6
0.3	180.5	150	120	0.8	—	—
0.4	202.8	186	880	4.5	—	—
0.6	223.4	191	1300	6.6	71.7	52.3
0.8	243.8	183	3100	13.4	—	—
1.0	267.9	191.2	3210	13.2	92.7 [10]	16.8 [12]

alous heat capacity, the parts of the temperature dependence of the total heat capacity $C_p(T)$, which were far from the phase transition region and represented the regular part C_{reg} of the heat capacity, were approximated by a polynomial. The anomalous contribution was determined as $\Delta C_p = C_p - C_{\text{reg}}$. It can be seen from Fig. 2 that the behavior of the heat capacity and the anomalies depend on the concentration ratio of the central atoms. The main quantitative thermodynamic parameters are given in the table. The parent compound $(\text{NH}_4)_2\text{WO}_2\text{F}_4$ is characterized by a loss of stability of the parent phase (space group $Cmcm$) at the temperature $T_1 = 201$ K, which is in good agreement with that data obtained in our previous investigations [6]. In the initial stage of the substitution for the central atom $\text{Mo} \rightarrow \text{W}$ ($x \leq 0.3$), we observed a decrease in the temperature T_1 and a decrease in the total enthalpy $\Sigma\Delta H_i$, which is associated with the sequence of phase transitions and determined by the integration of the anomalous heat capacity $\Delta C_p(T)$. The

$(\text{NH}_4)_2\text{W}_{0.7}\text{Mo}_{0.3}\text{O}_2\text{F}_4$ solid solution is characterized by the minimum value of the total enthalpy $\Sigma\Delta H_i \approx 120$ J/(mol K), which was found to be almost 25 times less than the value determined for the parent compound $(\text{NH}_4)_2\text{WO}_2\text{F}_4$ (see table). With a further increase in the molybdenum concentration ($x > 0.3$) the temperature of the structural phase transition $Cmcm \rightarrow Pnma$ increases to the temperature $T_1 = 270$ K, which is characteristic of $(\text{NH}_4)_2\text{MoO}_2\text{F}_4$ [10]; in this case, the total enthalpy also increases. The character of the change in the total entropy follows the behavior of the total enthalpy $\Sigma\Delta H_i(x)$. The change in the temperature between the distorted phases has a less pronounced dependence on the molybdenum concentration.

The thermal expansion of the crystals was measured on a NETZSCH DIL-402C dilatometer at temperatures in the range from 120 to 350 K in the dynamic regime at a heating rate of ~ 3 K/min. The experiments were performed in a helium flow-through atmosphere at a flow rate of ~ 50 mL min^{-1} . In order to calibrate the dilatometer and take into account the thermal expansion of the measurement system, we used reference samples from fused silica. The samples of the oxyfluorides under investigation were prepared in the form of pellets with a diameter of 8 mm and a height of ~ 4 –6 mm only by pressing under a pressure of ~ 2 GPa. We could not prepare ceramic samples according to the conventional technology, because they contained ammonia, which made impossible high-temperature sintering. The correctness of the use of uncalcined samples in the experiments was confirmed by a satisfactory agreement between the temperature dependences of the volume strain and the volume thermal expansion coefficient of the single-crystal and quasi-ceramic oxyfluorides $(\text{NH}_4)_2\text{WO}_2\text{F}_4$ (Fig. 3).

The results of measurements of the temperature dependences of the volume strain over a wide temperature range are presented in Fig. 4 for the parent compounds $(\text{NH}_4)_2\text{WO}_2\text{F}_4$, $(\text{NH}_4)_2\text{MoO}_2\text{F}_4$, and three solid solutions with molybdenum concentrations $x =$

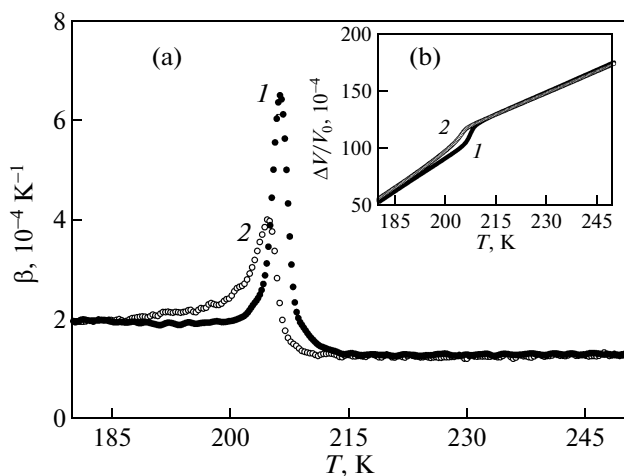


Fig. 3. Dependences (a) $\beta(T)$ and (b) $\Delta V/V_0(T)$ for (1) single-crystal sample and (2) quasi-ceramic sample of the $(\text{NH}_4)_2\text{WO}_2\text{F}_4$ oxyfluoride.

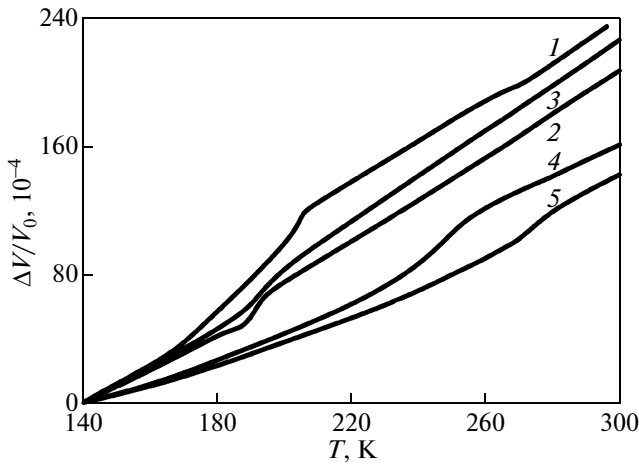


Fig. 4. Temperature dependences of the volume strain for (1) $(\text{NH}_4)_2\text{WO}_2\text{F}_4$; (2–4) $(\text{NH}_4)_2\text{W}_{1-x}\text{Mo}_x\text{O}_2\text{F}_4$ with $x = (2) 0.1, (3) 0.3,$ and (4) 0.8; and (5) $(\text{NH}_4)_2\text{MoO}_2\text{F}_4$.

0.2, 0.3, and 0.8. The rate of increase in the volume strain $\Delta V/V_0$ with an increase in the temperature decreases with an increase in the molybdenum concentration (curves 1, 2, 4, and 5 in Fig. 4). However, the exception is the $(\text{NH}_4)_2\text{W}_{0.7}\text{Mo}_{0.3}\text{O}_2\text{F}_4$ compound (curve 3 in Fig. 4), for which the average value $d(\Delta V/V_0)/dT$ in the temperature range from 140 to 300 K is larger than that for the sample with a molybdenum concentration $x = 0.2$. This specific feature, as will be shown below, also exhibits itself in the behavior of the other properties. We return to the discussion of this feature in the further when comparing the influences of the chemical and hydrostatic pressures.

For all the samples under investigation, we revealed anomalies in the behavior of the volume strain $\Delta V/V_0$ near the temperatures of the two-phase transitions, which were determined earlier in the DSM experiments. The anomalous behavior more clearly exhibits itself in the temperature dependences of the coefficients of volume thermal expansion (Fig. 5).

The susceptibility of the oxyfluorides to hydrostatic pressure was investigated using the differential thermal analysis (DTA) with a copper–germanium thermocouple as a working element. Powder samples weighing as much as 0.02–0.03 g were packed in a copper container attached to one of the junctions of the thermocouple. The working element was placed in a high-pressure chamber of the piston–cylinder type filled with silicone oil. The pressure coefficients dT/dp were measured in two solid solutions with molybdenum concentrations $x = 0.2$ and 0.6. The experimental procedure used in these measurements was similar to that described in [13].

The results of the performed measurements, together with our previous data on the pressure coefficients for the initial crystals [7, 10], are presented in the temperature–pressure phase diagrams (Fig. 6) and in

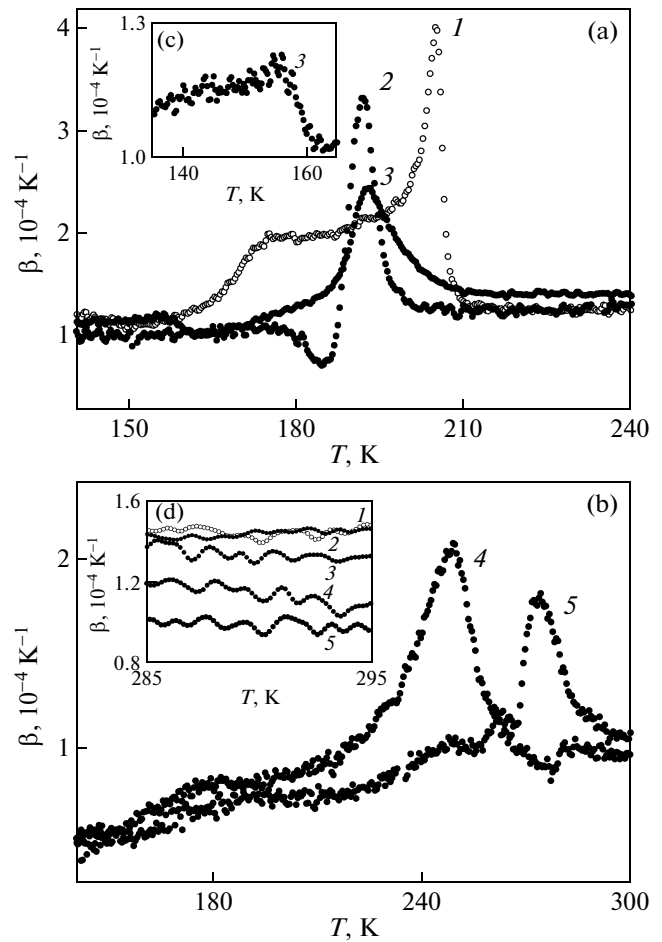


Fig. 5. Temperature dependences of the volume thermal expansion coefficient (a, b) over a wide temperature range and (d) near $T \approx 290$ K for (1) $(\text{NH}_4)_2\text{WO}_2\text{F}_4$; (2, 3) $(\text{NH}_4)_2\text{W}_{1-x}\text{Mo}_x\text{O}_2\text{F}_4$ with $x = (2) 0.2, (3) 0.3$ and (4) 0.8; and (5) $(\text{NH}_4)_2\text{MoO}_2\text{F}_4$. Inset (c) shows the function $\beta(T)$ for $(\text{NH}_4)_2\text{W}_{0.7}\text{Mo}_{0.3}\text{O}_2\text{F}_4$ in the vicinity of the temperature T_2 .

the table. For greater clarity, the changes in the phase transition temperatures T_i as a function of the concentration of the components and the pressure, are considered in Fig. 6 with respect to the temperatures T_1 and T_2 , which are characteristic of the parent compound $(\text{NH}_4)_2\text{WO}_2\text{F}_4$ ($(T/T_1)_{p=0} = 1$ and $(T/T_2)_{p=0} = 1$).

The positive values of dT_1/dp , which are almost constant in the pressure range under investigation, indicate a narrowing of the temperature region of the existence of the parent phase (space group $Cmcm$) in all the studied compounds (Fig. 6a). For example, the pressure coefficient dT_1/dp for the $(\text{NH}_4)_2\text{W}_{0.4}\text{Mo}_{0.6}\text{O}_2\text{F}_4$ oxyfluoride is significantly higher than that for the initial tungsten compound and approaches the value obtained for the molybdenum oxyfluoride $(\text{NH}_4)_2\text{MoO}_2\text{F}_4$ (see table). However, in this case, also, there is an exception, namely, in the

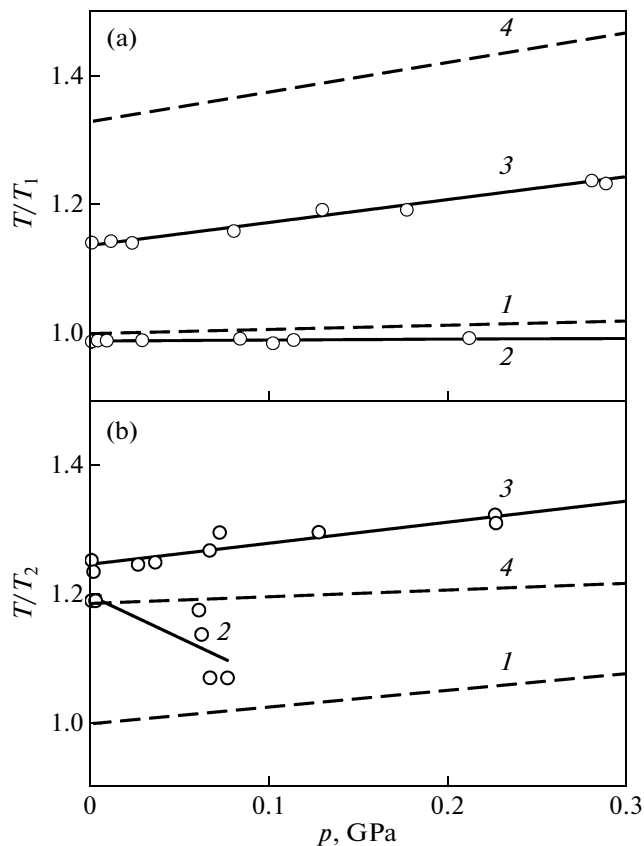


Fig. 6. Temperature–pressure phase diagrams in the vicinity of the temperatures (a) T_1 and (b) T_2 for (1) $(\text{NH}_4)_2\text{WO}_2\text{F}_4$; (2, 3) $(\text{NH}_4)_2\text{W}_{1-x}\text{Mo}_x\text{O}_2\text{F}_4$ with $x =$ (2) 0.2 and (3) 0.6; and (4) $(\text{NH}_4)_2\text{MoO}_2\text{F}_4$.

initial stage of the substitution $\text{Mo} \rightarrow \text{W}$, the pressure coefficient dT_1/dp decreases and, at the molybdenum concentration $x = 0.2$, becomes considerably smaller than that for the parent oxyfluoride $(\text{NH}_4)_2\text{WO}_2\text{F}_4$.

It can be seen from Fig. 6b and the table that there is no strict regularity in the dependence of the pressure coefficient dT_2/dp on the molybdenum concentration x . In particular, the stability of first distorted phases in the compounds with $x = 0, 0.6$, and 1.0 decreases with an increase in the pressure ($dT_1/dp > 0$), even though not systematically, whereas the susceptibility to hydrostatic pressure for the $(\text{NH}_4)_2\text{W}_{0.8}\text{Mo}_{0.2}\text{O}_2\text{F}_4$ solid solution is negative and rather high. Furthermore, with an increase in the pressure, the DTA anomaly at the temperature T_2 rapidly decreases and, at a pressure $p \sim 0.08$ GPa, is not observed at all.

The specific features revealed in the behavior of some properties of the samples with small molybdenum concentrations x stimulated the investigation of the heat capacity of the $(\text{NH}_4)_2\text{W}_{0.7}\text{Mo}_{0.3}\text{O}_2\text{F}_4$ solid solution with the use of adiabatic calorimetry. The measurements were performed under conditions of discrete ($\Delta T = 1\text{--}2$ K) and continuous ($dT/dt = 0.02\text{--}$

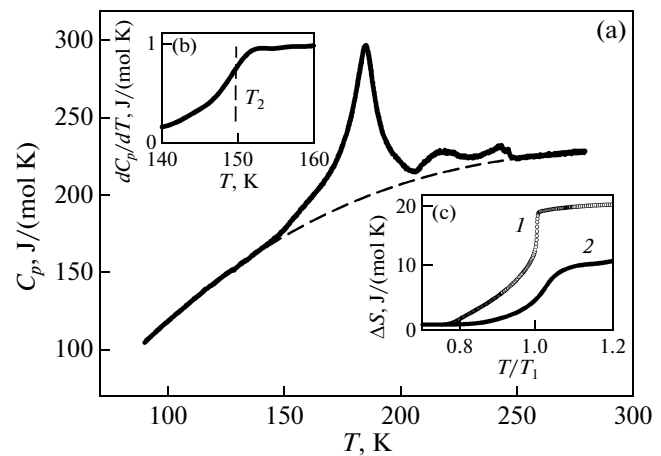


Fig. 7. Temperature dependences of (a) the molar heat capacity for $(\text{NH}_4)_2\text{W}_{0.7}\text{Mo}_{0.3}\text{O}_2\text{F}_4$ and (c) the anomalous entropy for (1) $(\text{NH}_4)_2\text{WO}_2\text{F}_4$ and (2) $(\text{NH}_4)_2\text{W}_{0.7}\text{Mo}_{0.3}\text{O}_2\text{F}_4$. Inset (b) shows the function dC_p/dT in the vicinity of the temperature T_2 .

0.20 K/min) heatings according to the procedure described in [14]. The test sample weighing as much as 0.28 g was hermetically packed in an aluminum container, whose heat capacity was determined in a separate experiment.

The temperature dependence of the molar heat capacity is shown in Fig. 7a. In contrast to the DSM data (see table), the anomalous behavior of the heat capacity is observed at four temperatures: $T_1 = 181.4 \pm 0.1$ K, $T_2 = 150 \pm 1$ K, $T'_1 = 216 \pm 1$ K, and $T'_2 = 242 \pm 1$ K. However, for the reliable measurement of the temperature T_2 , we had to consider the function dC_p/dT (Fig. 7b). The obtained values of T_1 and T_2 are in satisfactory agreement with temperatures at which the thermal expansion coefficients exhibit specific features. It is difficult to say anything about the nature of the heat capacity anomalies at the temperatures T'_1 and T'_2 , because, in this temperature range, no anomalous behavior was observed in the temperature dependence of the thermal expansion coefficient and, as will be seen below, in the temperature dependence of the birefringence.

The molar heat capacity was separated into the regular and anomalous components according to the same procedure as was used in the processing of the DSM data (see above). The anomalous heat capacity $\Delta C_p(T)$ is observed in the temperature range 140–250 K (Fig. 7a). However, because we unaware of the nature of the anomalies at the temperatures T'_1 and T'_2 , the changes in the total enthalpy $\Sigma \Delta H_i = 1800 \pm 80$ J/mol and the total entropy $\Sigma \Delta S_i = 10.4$ J/(mol K), which are associated with the sequence of phase tran-

sitions at the temperatures T_1 and T_2 , were determined in the temperature range from 140 to 210 K.

A comparison of the temperature dependences of the anomalous entropy for the $(\text{NH}_4)_2\text{W}_{0.7}\text{Mo}_{0.3}\text{O}_2\text{F}_4$ and $(\text{NH}_4)_2\text{WO}_2\text{F}_4$ compounds is presented in Fig. 7c. It can be seen from this figure that the substitution $\text{Mo} \rightarrow \text{W}$ leads to a significant decrease in the entropy associated with the sequence of phase transitions at the temperatures T_1 and T_2 . The high-temperature phase transition proved to be susceptible to the rate of measurement of the heat capacity $C_p(T)$ in series of continuous heatings. A change in the quantity dT/dt from 0.02 to 0.20 K/min led to an increase in the temperature of stability of the parent phase (space group $Cmcm$) by almost 3 K. Thus, the phase transition at the temperature T_1 in the solid solution remained a first-order transformation.

4. OPTICAL AND DIELECTRIC INVESTIGATIONS

The temperature dependences of the birefringence $\Delta n(T)$ were measured using the method of a Berek compensator (Leica) on an Axioskop-40 polarizing microscope with a Linkam LTS-350 thermal camera.

According to [1, 2], the $(\text{NH}_4)_2\text{MoO}_2\text{F}_4$ and $(\text{NH}_4)_2\text{WO}_2\text{F}_4$ single crystals have a plate-like habit with the smallest size along the [010] crystallographic direction and possess a perfect (010) cleavage plane. Since the most high-quality single crystals of the $(\text{NH}_4)_2\text{W}_{1-x}\text{Mo}_x\text{O}_2\text{F}_4$ solid solutions had small linear dimensions ($\sim 100 \mu\text{m}$), the selection of samples for our experiments and their orientation were performed according to the natural faceting. The birefringence was measured on the (010) plates with a thickness ranging from 45 to 90 μm .

The temperature dependences of the birefringence $\Delta n_b(T)$ for the samples with molybdenum concentrations $x = 0.2, 0.3,$ and 0.4 are shown in Fig. 8 by curves 2–4, respectively. The dependences $\Delta n_b(T)$ in the temperature range 270–370 K for the initial crystals $(\text{NH}_4)_2\text{MoO}_2\text{F}_4$ and $(\text{NH}_4)_2\text{WO}_2\text{F}_4$ have an identical linear behavior. At room temperature, the values of the birefringence are close to each other and lie in the range $\Delta n_b = 0.014\text{--}0.015$ [6, 9]. Below the temperature of the structural phase transition from the parent phase (space group $Cmcm$), the temperature dependences of the birefringence have different behaviors. In the $(\text{NH}_4)_2\text{WO}_2\text{F}_4$ oxyfluoride, the structural phase transition at the temperature $T_1 = 202 \text{ K}$ is accompanied by the change in the symmetry $Cmcm \leftrightarrow P\bar{1}$, which, in turn, leads to a decrease in the birefringence $\Delta n_b(T)$ below the temperature T_1 (Fig. 8, curve 1) [6]. In the $(\text{NH}_4)_2\text{WO}_2\text{F}_4$ compound, the structural phase transition at the temperature $T_1 \approx 267 \text{ K}$ is accompanied by the change in the symmetry

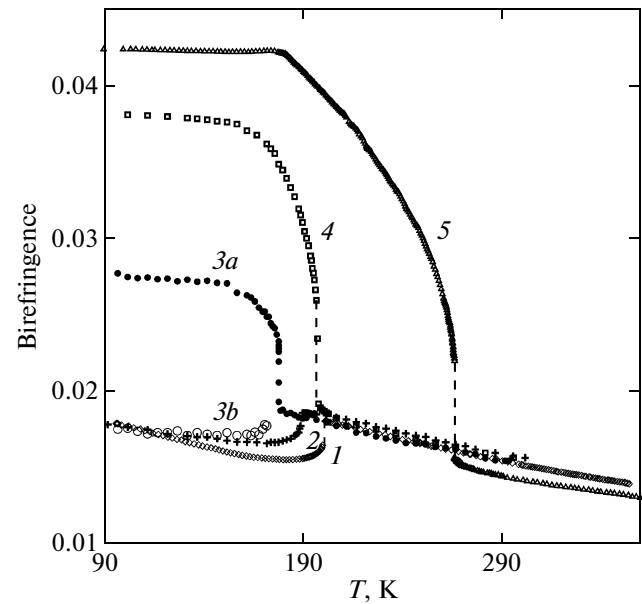


Fig. 8. Temperature dependences of the birefringence for (1) $(\text{NH}_4)_2\text{WO}_2\text{F}_4$; (2–4) $(\text{NH}_4)_2\text{W}_{1-x}\text{Mo}_x\text{O}_2\text{F}_4$ with $x =$ (2) 0.2, (3a, 3b) 0.3, and (4) 0.4; and (5) $(\text{NH}_4)_2\text{MoO}_2\text{F}_4$.

$Cmcm \leftrightarrow Pnma$, while the birefringence abruptly increases. At temperatures below T_1 , the birefringence Δn_b nonlinearly increases with a rather high rate. At the temperature T_2 , the curve $\Delta n_b(T)$ has a sharp inflection and, with a further decrease in the temperature, the birefringence continues to increase but considerably more slowly and almost linearly (Fig. 8, curve 5) [9]. Therefore, the symmetry of the low-temperature phase in the studied solid solutions $(\text{NH}_4)_2\text{W}_{1-x}\text{Mo}_x\text{O}_2\text{F}_4$ can be indirectly judged from the behavior of the temperature dependence of the birefringence.

The behavior of the function $\Delta n_b(T)$ for the compound with a molybdenum concentration $x = 0.2$ is similar to that for the parent compound $(\text{NH}_4)_2\text{WO}_2\text{F}_4$, even though there is a small decrease in the birefringence $\Delta n_b(T)$ below the temperature $T_1 = 190 \text{ K}$ (Fig. 8, curve 2).

In the case of the solid solution with a molybdenum concentration $x = 0.4$, the dependence $\Delta n_b(T)$ is identical to that observed for the parent compound $(\text{NH}_4)_2\text{MoO}_2\text{F}_4$ (Fig. 8, curve 4); i.e., in this crystal, there occurs a structural phase transition with the change in the symmetry $Cmcm \leftrightarrow Pnma$ and the jump in the birefringence at the phase transition point. The phase transition at the temperature T_2 is less pronounced, but, nonetheless, it still takes place at $\sim 185 \text{ K}$. The birefringence Δn_b decreases at temperatures $T < T_2$ by approximately 11% as compared to the molybdenum compound.

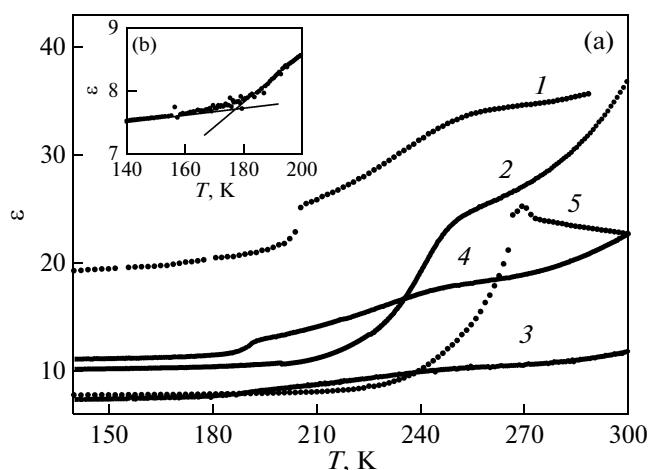


Fig. 9. (a) Temperature dependences of the permittivity for (1) $(\text{NH}_4)_2\text{WO}_2\text{F}_4$; (2–4) $(\text{NH}_4)_2\text{W}_{1-x}\text{Mo}_x\text{O}_2\text{F}_4$ with $x = (2) 0.2, (3) 0.3,$ and $(4) 0.8$; and (5) $(\text{NH}_4)_2\text{MoO}_2\text{F}_4$. Inset (b) shows the function $\varepsilon(T)$ for $(\text{NH}_4)_2\text{W}_{0.7}\text{Mo}_{0.3}\text{O}_2\text{F}_4$ in the vicinity of the temperature T_1 .

For the $(\text{NH}_4)_2\text{W}_{0.7}\text{Mo}_{0.3}\text{O}_2\text{F}_4$ solid solution at temperatures above $T_1 = 180$ K, the birefringence has a linear temperature dependence. Below this temperature, there are two regions where the dependences $\Delta n_b(T)$ differ significantly: in one region, the behavior of the birefringence is characteristic of the structural phase transition $Cmcm \leftrightarrow Pnma$, whereas in the other region, it is characteristic of the structural phase transition $Cmcm \leftrightarrow P\bar{1}$ (Fig. 8, curves 3a and 3b, respectively).

The temperature dependences of the permittivity of the solid solutions with molybdenum concentrations $x = 0.2, 0.3,$ and 0.8 were investigated using an E7-20 immittance meter at a frequency of 1 kHz in the temperature range from 100 to 320 K. The measurements were performed on the samples with a diameter of 8 mm and a height of 1–2 mm, which were prepared according to the same technique as was used for samples in the thermal expansion investigations. In our previous work [15], we showed that the behavior of the dependence $\varepsilon(T)$ measured on a “quasi-ceramic” sample for the parent compound $(\text{NH}_4)_2\text{WO}_2\text{F}_4$ is in satisfactory agreement with the temperature dependence of the arithmetic mean of the permittivities along the principal crystallographic directions of the single-crystal sample, i.e., $(\sum \varepsilon_i/3)(T)$. For the permittivity measurements, the electrodes were prepared by vacuum deposition of gold onto the samples. The rates of change in the temperature during heating and cooling were equal to ~ 0.7 K/min.

The $(\text{NH}_4)_2\text{WO}_2\text{F}_4$ compound has the highest values of the permittivity over the entire temperature range under investigation (Fig. 9a, curve 1). The substitution $\text{Mo} \rightarrow \text{W}$ results in a gradual decrease in the

permittivity. The behavior of the temperature dependence $\varepsilon(T)$ for the compound with a molybdenum concentration $x = 0.2$ (Fig. 9a, curve 2) is similar to the behavior of the dependence $\varepsilon(T)$ for the parent compound $(\text{NH}_4)_2\text{WO}_2\text{F}_4$, with the only difference that, at the temperature T_1 , the jump in the permittivity decreases by a factor of two. For the $(\text{NH}_4)_2\text{W}_{0.2}\text{Mo}_{0.8}\text{O}_2\text{F}_4$ solid solution, the dependence $\varepsilon(T)$ is qualitatively similar to that observed in the $(\text{NH}_4)_2\text{MoO}_2\text{F}_4$ compound (Fig. 9a, curves 4 and 5, respectively), and the jump in the permittivity at the phase transition point decreases only slightly ($\Delta\varepsilon \approx 15$).

A significantly different behavior of the permittivity is observed in the solid solution with a molybdenum concentration $x = 0.3$ (Fig. 9a, curve 3). In the low-temperature region, the permittivity ε of this compound proved to be 6% lower than that of the $(\text{NH}_4)_2\text{MoO}_2\text{F}_4$ compound. At the temperature $T_1 \approx 180$ K, the dielectric anomaly in the $(\text{NH}_4)_2\text{W}_{0.7}\text{Mo}_{0.3}\text{O}_2\text{F}_4$ compound is very small and exhibits itself only with a change in the slope of the curve $\varepsilon(T)$ (Fig. 9b).

5. INFLUENCE OF THE SUBSTITUTION FOR THE CENTRAL ATOM ON THE STABILITY OF THE ORTHORHOMBIC STRUCTURE

The results obtained from detailed investigations of the thermal, physical, dielectric, optical, and structural properties of the oxyfluorides allow us to elucidate the character of the influence of the central atom on the mechanism and nature of phase transitions in the $(\text{NH}_4)_2\text{W}_{1-x}\text{Mo}_x\text{O}_2\text{F}_4$ solid solutions by analyzing the “phase transition temperature–composition” and “unit cell volume–composition” phase diagrams (Fig. 10).

The complete substitution $\text{Mo} \rightarrow \text{W}$ leads to an increase in the unit cell volume V_{uc} by 0.2%, i.e., $V_{uc} = 614.06(7) \text{ \AA}^3$ for $(\text{NH}_4)_2\text{WO}_2\text{F}_4$ and $V_{uc} = 615.48(1) \text{ \AA}^3$ for $(\text{NH}_4)_2\text{MoO}_2\text{F}_4$, as well as to a significant (by approximately 70 K) narrowing of the stability region of the parent phase (space group $Cmcm$). The specific feature observed in the dependence $V_{uc}(x)$ in the region of low molybdenum concentrations is more pronounced than the corresponding features in the concentration dependences of the unit cell parameters $a(x), b(x),$ and $c(x)$ (Figs. 10a and 1, respectively). For the molybdenum concentration $x = 0.2$, the unit cell volume of the solid solution decreases by approximately 0.3% as compared to the parent compound $(\text{NH}_4)_2\text{WO}_2\text{F}_4$. Summarizing the structural data, we can assume that the boundary between the distorted phases $P\bar{1}$ and $Pnma$, which are inherent in the parent oxyfluorides $(\text{NH}_4)_2\text{WO}_2\text{F}_4$ and $(\text{NH}_4)_2\text{MoO}_2\text{F}_4$, respectively, most likely lies in the molybdenum concentration region $x = 0.2–0.4$.

This assumption is confirmed by the results obtained from the analysis of the concentration dependences of the phase transition temperatures (Fig. 10b). The boundaries between the parent (space group $Cmcm$) and distorted phases (space groups $P\bar{1}$ and $Pnma$) are nonlinear and converge in the molybdenum concentration region $\sim 30\%$, which indicates the presence of a triple point in the $T-x$ phase diagram. It is here that, at the same temperature in different parts of one sample, there appear anomalous birefringences of opposite signs, which are characteristic of the tungsten and molybdenum oxyfluoride compounds. It should be noted that, regardless of the composition, the changes in the entropy ΔS_1 , including the triple point, proved to be characteristic of phase transitions of the order–disorder type. This means that, irrespective of their nature, the structural distortions occurring in the solid solutions under investigation are very significant.

For a molybdenum concentration $x < 0.3$, the solid solutions exhibit properties which are characteristic of the parent compound $(\text{NH}_4)_2\text{WO}_2\text{F}_4$. This is most clearly demonstrated by the behavior of the optical properties, as well as by the character of the susceptibility to hydrostatic pressure: the pressure coefficient dT_1/dp decreases with an increase in the molybdenum concentration. The latter circumstance is consistent with the data on the $T-p$ phase diagram of the tungsten compound, where in the range of negative pressures (i.e., with an increase in the unit cell volume V_{uc}), the temperature T_1 decreases [6]. However, a more rapid decrease in the temperature T_2 leads to a broadening of the temperature region of the existence of the distorted phase (space group $P\bar{1}$) at negative pressures. These data are in agreement with the results obtained from measurements of the pressure coefficients in the $(\text{NH}_4)_2\text{W}_{0.8}\text{Mo}_{0.2}\text{O}_2\text{F}_4$ solid solution, whose volume, even though only slightly, but is still larger than the volume of the $(\text{NH}_4)_2\text{WO}_2\text{F}_4$ solid solution (table, Fig. 10a). The behavior of the physical properties of the $(\text{NH}_4)_2\text{W}_{1-x}\text{Mo}_x\text{O}_2\text{F}_4$ compounds with molybdenum concentrations $x > 0.3$ is similar to that of the $(\text{NH}_4)_2\text{WO}_2\text{F}_4$ compound. This is evident from the behavior of the birefringence of the $(\text{NH}_4)_2\text{W}_{0.6}\text{Mo}_{0.4}\text{O}_2\text{F}_4$ compound (Fig. 8) and the pressure coefficients of the $(\text{NH}_4)_2\text{W}_{0.2}\text{Mo}_{0.8}\text{O}_2\text{F}_4$ compound (see table). Thus, it is clear that, upon distortion of the parent phase (space group $Cmcm$) due to the structural phase transition, the antiferroelectric state is more stable.

The changes observed in the temperatures of the phase transitions between the distorted phases $P\bar{1} \leftrightarrow ?$ and $Pnma \leftrightarrow ?$ are much less pronounced; however, the minimum in the dependence $T_2(x)$ also takes place in the region of $x \approx 0.3$. This can indicate the participation of the same structural elements or fragments in the

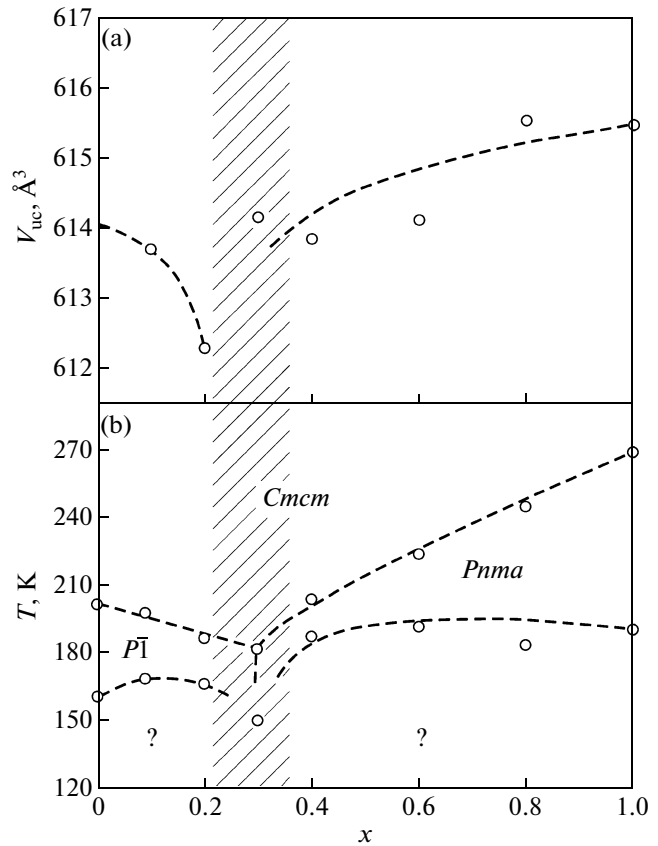


Fig. 10. (a) The unit cell volume–composition phase diagram and (b) the temperature–composition phase diagram.

mechanisms of both sequences of structural phase transitions $Cmcm \leftrightarrow P\bar{1} \leftrightarrow ?$ and $Cmcm \leftrightarrow Pnma \leftrightarrow ?$, which are characteristic of the tungsten and molybdenum oxyfluorides. And, this actually follows from the results of structural investigations [4, 5, 8, 16], which confirm the active role of the tetrahedral cations and sixfold-coordinated anions. The lack of data on the symmetry of the distorted phases below the temperature T_2 in the parent compounds does not allow us to make any assumptions about how in the phase diagram at low molybdenum concentrations they are related to the line of the structural phase transitions $P\bar{1} \leftrightarrow Pnma$.

6. CONCLUSIONS

A series of $(\text{NH}_4)_2\text{W}_{1-x}\text{Mo}_x\text{O}_2\text{F}_4$ solid solutions has been synthesized by means of the substitution for the central atom in the parent compounds $(\text{NH}_4)_2\text{WO}_2\text{F}_4$ and $(\text{NH}_4)_2\text{MoO}_2\text{F}_4$, which are characterized by an identical high-temperature structure (space group $Cmcm$) but with different types of disorder of fluorine–oxygen ligands and which undergo

structural phase transitions of the ferroelastic and antiferroelectric natures, respectively.

The performed investigations of the temperature dependences of the heat capacity, thermal expansion, permittivity, and birefringence, as well as the temperature–composition, unit cell volume–composition, and temperature–pressure phase diagrams, have made it possible to elucidate the character of the influence of the chemical and hydrostatic pressures on the boundaries of the regions of the existence of crystalline phases of different physical natures in the $(\text{NH}_4)_2\text{W}_{1-x}\text{Mo}_x\text{O}_2\text{F}_4$ oxyfluorides. It has been found that, in the same sample ($x = 0.3$), there coexist phases with the symmetries $P\bar{1}$ and $Pnma$, which are characterized by different behaviors of the optical properties but are formed at the same temperature. In accordance with the entropy parameters, the mechanism of structural distortions almost does not depend on the composition of the solid solutions.

It has been established that the more stable, i.e., energetically more favorable, state is the antiferroelectric state observed in the $(\text{NH}_4)_2\text{W}_{1-x}\text{Mo}_x\text{O}_2\text{F}_4$ solid solutions over a wide range of molybdenum concentrations ($x > 0.3$).

ACKNOWLEDGMENTS

We would like to thank G.V. Bondarenko for performing the X-ray fluorescence analysis.

This study was supported by the Russian Foundation for Basic Research (project no. 12-02-31566mol_a) and the Council on Grants from the President of the Russian Federation for Support of Leading Scientific Schools of the Russian Federation (project no. NSh-4828.2012.2).

REFERENCES

1. P. A. Maggard, T. S. Nault, C. L. Stern, and K. R. Poeppelmeier, *J. Solid State Chem.* **175**, 27 (2003).

2. M. R. Marvel, J. Lesage, J. Baek, P. S. Halasyamani, C. L. Stern, and K. R. Poeppelmeier, *J. Am. Chem. Soc.* **129**, 13963 (2007).
3. M. E. Welk, A. J. Norquist, C. L. Stern, and K. R. Poeppelmeier, *Inorg. Chem.* **40**, 5479 (2001).
4. A. A. Udovenko and N. M. Laptash, *Acta Crystallogr., Sect. B: Struct. Sci.* **64**, 645 (2008).
5. A. A. Udovenko, A. D. Vasiliev, and N. M. Laptash, *Acta Crystallogr., Sect. B: Struct. Sci.* **66**, 34 (2010).
6. S. V. Mel'nikova, V. D. Fokina, and N. M. Laptash, *Phys. Solid State* **48** (1), 117 (2006).
7. I. N. Flerov, V. D. Fokina, M. V. Gorev, A. D. Vasil'ev, A. F. Bovina, M. S. Molokeev, A. G. Kocharova, and N. M. Laptash, *Phys. Solid State* **48** (4), 759 (2006).
8. I. N. Flerov, V. D. Fokina, M. V. Gorev, E. V. Bogdanov, M. S. Molokeev, A. F. Bovina, and A. G. Kocharova, *Phys. Solid State* **49** (6), 1149 (2007).
9. S. V. Mel'nikova and N. M. Laptash, *Phys. Solid State* **50** (3), 511 (2008).
10. V. D. Fokina, E. V. Bogdanov, E. I. Pogorel'tsev, V. S. Bondarev, I. N. Flerov, and N. M. Laptash, *Phys. Solid State* **52** (1), 158 (2010).
11. E. V. Bogdanov, A. D. Vasil'ev, I. N. Flerov, and N. M. Laptash, *Phys. Solid State* **53** (2), 303 (2011).
12. M. V. Gorev, E. V. Bogdanov, I. N. Flerov, A. G. Kocharova, and N. M. Laptash, *Phys. Solid State* **52** (1), 167 (2010).
13. I. N. Flerov, M. V. Gorev, V. D. Fokina, A. F. Bovina, E. V. Bogdanov, E. I. Pogorel'tsev, and N. M. Laptash, *J. Fluorine Chem.* **132**, 713 (2011).
14. A. V. Kartashev, I. N. Flerov, N. V. Volkov, and K. A. Sablina, *Phys. Solid State* **50** (11), 2115 (2008).
15. I. N. Flerov, V. D. Fokina, A. F. Bovina, E. V. Bogdanov, M. S. Molokeev, A. G. Kocharova, E. I. Pogorel'tsev, and N. M. Laptash, *Phys. Solid State* **50** (3), 515 (2008).
16. L. S. Smirnov, A. I. Kolesnikov, I. N. Flerov, and N. M. Laptash, *Phys. Solid State* **51** (11), 2362 (2009).

Translated by O. Borovik-Romanova